*J. Fluid Mech.* (1989), *vol.* 200, *pp.* 337–365
*Printed in Great Britain*



# The effect of interaction on the boundary layer induced by a convected rectilinear vortex

By FU-SHENG CHUANG† AND A. T. CONLISK‡

† Department of Mechanical Engineering, National Taiwan Institute of Technology, Taipei, Taiwan, ROC

‡ Department of Mechanical Engineering, The Ohio State University, Columbus, OH 43210, USA

(Received 17 November 1987)

The effect of interaction on the boundary layer induced by a convected rectilinear vortex is considered. Two schemes are employed in the numerical discretization of the edge interaction condition; the first, developed by Veldman (1981) is useful at larger Reynolds numbers but fails to capture the interactive phase of the motion for Reynolds numbers less than $8 \times 10^4$. A scheme devised by Napolitano, Werlé & Davis (1978) is employed at smaller Reynolds numbers and yields similar results to Veldman's scheme at higher Reynolds numbers, while exhibiting greater numerical stability during the interactive phase of the motion. The effect of interaction is found to be negligible during much of the motion, even for a strong vortex, but during the latter stages of the calculations, interaction appears to round off the top of the eddy and delays breakdown for all Reynolds numbers studied when compared with the non-interactive results of Doligalski & Walker (1984). In addition, in the latter stages of the calculations, and during the early stages of the interactive phase, a third eddy is formed with vorticity of the same sign as the main eddy spawned deep within the boundary layer. Such a tertiary eddy has been observed in the experimental work of Walker *et al.* (1987) in their study of the boundary layer induced by a vortex ring. During the interactive phase of the motion a streamwise lengthscale emerges whose length is approximately $O(Re^{-\frac{3}{11}})$, broadly in line with the analytical predictions of Elliott, Cowley & Smith (1983). A novel feature of the computations is the use of a pseudospectral method (Burggraf & Duck 1982) in the streamwise direction which requires no special coding in reversed-flow regions.

## 1. Introduction

Inviscid flows containing vorticity occur in a wide variety of fluid motions; however, relatively little is known about how such flows interact with the viscous boundary layers which must be present on all solid walls in any real fluid. One such interaction can be observed between the trailing vortices produced at the tip of an aircraft wing and the boundary layer formed on the ground. The second example may be found in flows over submarines which may often encounter pockets of vorticity in the underwater environment.

The literature on this problem is extremely limited; experimentally, Harvey & Perry (1971) mounted a single wing in a wind tunnel to simulate the take-off or landing conditions of an aeroplane. The trailing vortex created at the wing tip was observed to induce a boundary-layer separation in the form of a secondary vortex. Theoretically, Doligalski & Walker (1984) and Walker (1978) conducted extensive

numerical studies on the boundary-layer flow induced by a rectilinear vortex and found that the boundary-layer motion was unsteady and the vortex induces a secondary vortex in the vicinity of the boundary, which eventually leads to a catastrophic breakdown of the boundary layer. In their study, conventional boundary-layer techniques were used, and the catastrophic breakdown of the boundary layer is manifested in a rapid growth in displacement thickness behind the vortex which eventually leads to failure of the numerical scheme. Recently, Walker *et al.* (1987) have observed the violent interaction between a vortex ring and the boundary layer on a horizontal wall; a similar set of experiments has also been performed by Nelson (1986).

In the present work we seek to extend the results of Doligalski & Walker to the case where there is interaction between the convected rectilinear vortex and the boundary-layer flow. In interacting-boundary-layer theory, the displacement thickness and the pressure distribution are coupled, unlike in conventional boundary-layer theory in which the pressure gradient is impressed on the boundary layer (see Burggraf 1982; Burggraf *et al.* 1979; Davis & Werle 1982; and Veldman 1981 for application to steady flow problems and Henkes & Veldman 1987 for the only application to unsteady flow problems of which the authors are aware).

A major result of the present work is that a third eddy appears to be spawned deep in the boundary layer next to (and of the same rotation as) the main boundary-layer eddy, indicative of the results of Walker *et al.* (1987) and Nelson (1986) for vortex rings. In this regard there are three major purposes of the present work. The first is to determine the effect of interaction between the vortex motion and the boundary layer on the breakdown phenomenon. The second purpose is to test a relatively new computational method, i.e. that of using the fast Fourier transform (FFT) in the streamwise direction, which is infinite. The method as applied here was first used by Burggraf & Duck (1982) in steady computations of flows past humps. In essence, the use of the FFT eliminates the need of special computational techniques to handle reversed-flow regions and is very efficient. In Burggraf & Duck's (1982) problem they found that larger size humps could be considered with fewer grid points in the streamwise direction when compared to standard finite-difference techniques.

The third purpose of the present work is to determine the effect of Reynolds number on the flow. The present problem is an example of a situation in which large-scale breakaway separation is expected to occur in which the boundary layer and inviscid flow interact strongly. Indeed, during the latter stages of the present calculations an interactive region is clearly delineated (a region that cannot be delineated from the classical boundary-layer calculations of Walker (1978) and Doligalski & Walker (1984)). It is natural to inquire, then, whether the spatial dimensions and temporal scaling of this region are consistent with the recent analytical work of Elliott, Cowley & Smith (1983) in which the streamwise scale of the interactive region is $O(Re^{-\frac{3}{11}})$ and the timescale is $O(Re^{-\frac{2}{11}})$ (see §5 of that work) where $Re$ is the Reynolds number. Our results, it turns out, are broadly in line with the spatial scaling based on the calculated results for several values of Reynolds number.

To fix ideas, the flow problem of current interest is the boundary-layer flow induced by a convected rectilinear vortex which is outside the boundary layer. Two types of bounding surfaces will be considered in this paper: one is a plane surface, the other a plane surface with a small hump. A novel feature of this work as mentioned previously is that interaction between the inviscid flow and the boundary layer flow is incorporated. The flow is assumed to be laminar and two-dimensional and the

dimensionless displacement thickness is assumed small and of order of $Re^{-\frac{1}{2}}$. In the present study, separation of the boundary layer is expected for cases of large vortex strength. Consequently the displacement thickness will increase drastically around the separation region.

Both the results of non-interacting and interacting theory will be analysed and compared. The development of streamline patterns with respect to time will be presented for different vortex strengths, as in Doligalski & Walker (1984). The development of the interaction region will be examined and the results compared with the scales deduced by Elliott *et al.* (1983); both a plane wall and flow past a hump will be examined. It should be noted that the only other apparent application of interacting-boundary-layer theory to a problem of this type is that of Henkes & Veldman (1987) who considered the boundary-layer flow past an impulsively started cylinder at several Reynolds numbers from $10^4$–$10^6$. As noted by Van Dommelen (1981) and others this flow breaks down due to the separation of the boundary layer and subsequent start of the vortex shedding process. The results of Henkes & Veldman (1987) indicate that interaction does at least delay the breakdown process if not eliminating it altogether. A similar result is obtained with the present calculations; it will be shown that, depending on vortex strength, the calculations may be continued significantly beyond the non-interacting case. In fact, it is this continuation in the calculations that enables the streamwise scale of the strong interaction region of Elliott *et al.* (1983) to be identified.

The plan of the paper is as follows; in §2, the boundary layer and inviscid flow problems are formulated; the inviscid flow solution which consists of the potential flow due to the vortex in a uniform stream and an $O(Re^{-\frac{1}{2}})$ component due to the displacement thickness is given and the starting conditions are discussed. In §3 the numerical methods are discussed, and the results for both the plane wall and a hump are presented in §4 for $Re = 8 \times 10^4$. The effect of Reynolds number on the calculations is discussed in §5 and conclusions are presented in §6.

## 2. Formulation

### 2.1. *The boundary-layer problem*

The problem can be defined as follows. A rectilinear vortex convects in a uniform flow of speed $U_\infty$ above a plane wall (figure 1*a*) or a plane boundary with small hump (figure 1*b*). In both cases, a boundary layer will develop on the surface. The boundary-layer problem is coupled with the inviscid flow via a pressure-displacement relation within the interacting-boundary-layer concept. The plane boundary case will be considered first.

The governing equations for this problem are the boundary-layer equations, which are given by

$$\rho\left(\frac{\partial u^*}{\partial t^*}+u^*\frac{\partial u^*}{\partial x^*}+v^*\frac{\partial u^*}{\partial y^*}\right)=-\frac{\partial p^*}{\partial x^*}+\mu\frac{\partial^2 u^*}{\partial y^{2*}}, \tag{1}$$

$$\frac{\partial u^*}{\partial x^*}+\frac{\partial v^*}{\partial y^*}=0, \tag{2}$$

where $u^*, v^*$ are flow velocities in the $x^*$ and $y^*$ directions respectively, $\rho$ is the constant density of the flow medium, $p^*$ is the pressure in the flow field, and $\mu$ is the viscosity of the medium.

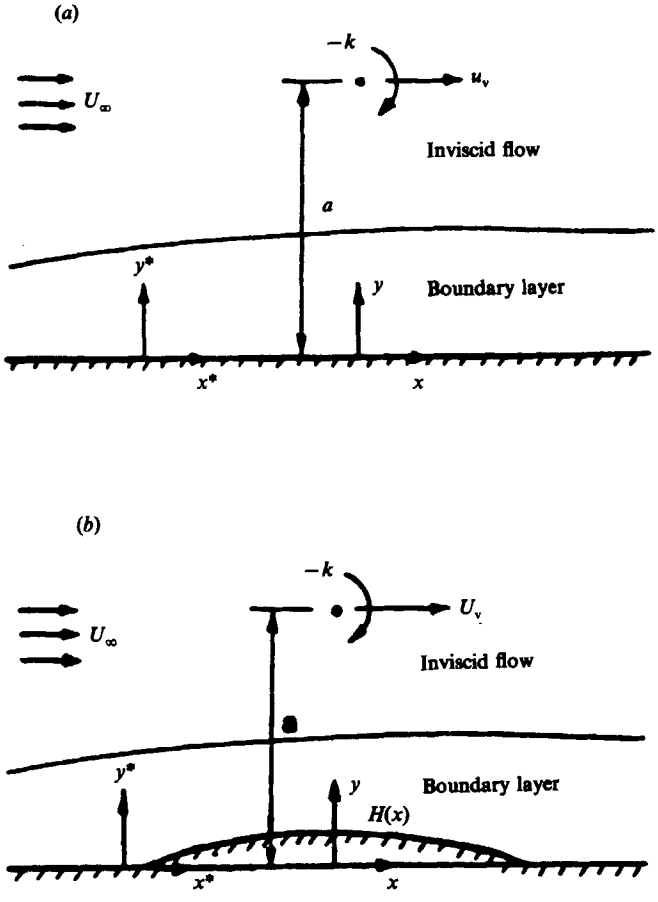


FIGURE 1. Schematic of the present problem; vortex above (*a*) a plane wall, and (*b*) a plane wall with a small hump.

The equations can be transformed into the dimensionless form by defining the following dimensionless boundary-layer variables:

$$\left.\begin{aligned} \bar{x} = \frac{x^*}{a}, \quad y = \frac{y^*}{a} Re^{\frac{1}{2}}, \quad t = \frac{t^*}{a/U_\infty}, \quad k = \frac{k^*}{aU_\infty}, \\ u = \frac{u^*}{U_\infty}, \quad v = \frac{v^*}{U_\infty} Re^{\frac{1}{2}}, \quad p = \frac{p^*}{\frac{1}{2}\rho U_\infty^2}, \end{aligned}\right\} \tag{3}$$

where $a$ is the vertical distance of the vortex from the plane boundary at time $t = 0$ as shown in figure 1 and $k^*$ is the dimensional vortex strength.† $Re = U_\infty a/\nu$ is the Reynolds number and $U_\infty$ is the free-stream speed at $\bar{x} = \pm\infty$. Substituting these relationships into (1) and (2), the non-dimensional form of the governing equations

† Note that this non-dimensionalization is somewhat different from that of Doligalski & Walker (1984). In that work all velocities are non-dimensionalized on $(1-\alpha)U_\infty$, where $\alpha$ is the non-interacting vortex speed (see below) and the vortex strength $\kappa$ in that work corresponds to $-k^*/2\pi$ here.

in the inertial frame become

$$\frac{\partial u}{\partial t}+u\frac{\partial u}{\partial \bar{x}}+v\frac{\partial u}{\partial y}=-\frac{\partial p}{\partial \bar{x}}+\frac{\partial^2 u}{\partial y^2}, \tag{4a}$$

$$\frac{\partial u}{\partial \bar{x}}+\frac{\partial v}{\partial y}=0. \tag{4b}$$

Equations (4) are subject to the initial and boundary conditions

$$u, v \quad \text{specified at} \quad t=0, \tag{5a}$$

$$u, v \quad \text{specified as} \quad \bar{x}\to\pm\infty, \tag{5b}$$

$$u=v=0 \quad \text{at} \quad y=0, \tag{5c}$$

$$u\to U_{\mathrm{e}}(\bar{x},t) \quad \text{as} \quad y\to\infty, \tag{5d}$$

where the inviscid slip velocity $U_{\mathrm{e}}$ is given from interacting boundary-layer theory (Burggraf *et al.* 1979) as

$$U_{\mathrm{e}}(\bar{x},t)=U_{\mathrm{I}}(\bar{x},t)+\frac{1}{\pi Re^{\frac{1}{2}}}\int_{-\infty}^{\infty}\frac{\partial}{\partial\xi}(U_{\mathrm{e}}\delta^*)\frac{\mathrm{d}\xi}{\bar{x}-\xi}, \tag{6}$$

and the displacement $\delta^*$ is defined by

$$U_{\mathrm{e}}\delta^*(\bar{x},t)=\int_0^{\infty}(U_{\mathrm{e}}-u)\,\mathrm{d}y. \tag{7}$$

Here, $U_{\mathrm{I}}$ is the edge velocity induced by the inviscid flow corresponding to a single vortex above a plane wall and is given by (Milne-Thompson 1960) as

$$U_{\mathrm{I}}(\bar{x},t)=1+\frac{k}{\pi}\frac{y_{\mathrm{v}}(t)}{(\bar{x}-x_{\mathrm{v}}(t))^2+y_{\mathrm{v}}^2(t)}, \tag{8}$$

where $(x_{\mathrm{v}}, y_{\mathrm{v}})$ is the vortex position. Within the interacting boundary-layer concept, the pressure gradient term in (4*a*) must be calculated at each time-step; using the Euler equation the pressure gradient is given by

$$-\frac{\partial p}{\partial \bar{x}}=\frac{\partial U_{\mathrm{e}}}{\partial t}+U_{\mathrm{e}}\frac{\partial U_{\mathrm{e}}}{\partial \bar{x}}. \tag{9}$$

It should be noted here that for the classical boundary-layer problem, posed by Doligalski & Walker (1984), it is easily seen that $y_{\mathrm{v}}(t)=$ constant $=y_{\mathrm{v}}(0)=1$ and

$$\frac{\mathrm{d}x_{\mathrm{v}}(t)}{\mathrm{d}t}=1+\frac{k}{4\pi}=\alpha=\text{constant}. \tag{10}$$

Consequently, $x_{\mathrm{v}}(t)=\alpha t$ and hence, in a frame of reference travelling with the vortex the inviscid surface speed $U_{\mathrm{e}}=U_{\mathrm{I}}(x)$ and is independent of time; nevertheless, the boundary layer is inherently unsteady.

For the present study, it is necessary to specify an initial condition. Because the principal interest is in the terminal nature of the boundary-layer flow induced by a convected vortex and for comparison with the results of Doligalski & Walker (1984), their initial state is used in this study. The plane boundary is assumed to be

introduced into the already existing uniform and vortex flow field; in other words, the effect of viscosity can be imagined to be suddenly present at $t = 0$ and the flow field is similar to a Rayleigh boundary layer. Moreover, because the effect of the vortex will diminish at points far away from the vortex, the problem then becomes the boundary-layer problem of a uniform flow over a suddenly present plane boundary. Hence the solution of the current problem as $\bar{x} \to \pm\infty$, can be described as

$$U_{\mathrm{R}} = \mathrm{erf}\,(y/2t^{\frac{1}{2}}) \tag{11}$$

where erf denotes the Error Function.

Equation (11) suggests that a Rayleigh transformation $\eta = y/2t^{\frac{1}{2}}$ is appropriate; also, transforming the equation to a coordinate system convecting at the speed of the vortex in the $\bar{x}$-direction given by $x = \bar{x} - x_{\mathrm{v}}(t)$, the governing equations (4) become

$$\left.\begin{aligned} 4t\frac{\partial\tilde{u}}{\partial t} - 2\eta\frac{\partial\tilde{u}}{\partial\eta} + 4t(U_{\mathrm{R}} - U_{\mathrm{v}})\frac{\partial\tilde{u}}{\partial x} - \frac{\partial^2\tilde{u}}{\partial\eta^2} \\ = -4t\frac{\partial p}{\partial x} - 2t^{\frac{1}{2}}v\frac{\partial U_{\mathrm{R}}}{\partial\eta} - 4t\tilde{u}\frac{\partial\tilde{v}}{\partial x} - 2t^{\frac{1}{2}}v\frac{\partial\tilde{u}}{\partial\eta}, \\ 2t^{\frac{1}{2}}\frac{\partial\tilde{u}}{\partial x} + \frac{\partial v}{\partial\eta} = 0, \end{aligned}\right\} \tag{12}$$

where $\tilde{u}$ is defined by

$$u(x, y, t) = U_{\mathrm{R}}(\eta) + \tilde{u}(x, \eta, t),$$

and $U_{\mathrm{R}}$ is given by (11). Equations (12) are subject to the boundary conditions

$$\left.\begin{aligned} &\tilde{u} = v = 0 \quad \text{at} \quad \eta = 0, \\ &\tilde{u} \to 0 \quad \text{as} \quad x \to \pm\infty, \\ &\tilde{u} \to \tilde{U}_{\mathrm{e}}(x, t) \quad \text{as} \quad \eta \to \infty, \end{aligned}\right\} \tag{13}$$

where $\tilde{U}_{\mathrm{e}} = U_{\mathrm{e}} - 1$. The initial condition is obtained by solving (12) as $t \to 0$; the methodology is standard and the solution is given by Doligalski & Walker (1984) for several terms in a perturbation series in $t^{\frac{1}{2}}$, and the result for the initial condition is given by

$$u = \tilde{U}_{\mathrm{I}}(x, 0)\, U_{\mathrm{R}}(\eta) \quad \text{at} \quad t = 0, \tag{14}$$

where $\tilde{U}_{\mathrm{I}}(x, 0) = U_{\mathrm{I}}(x, 0) - 1$. Finally, the Euler equation for the pressure gradient becomes

$$-\frac{\partial p}{\partial x} = \frac{\partial\tilde{U}_{\mathrm{e}}}{\partial t} + (\tilde{U}_{\mathrm{e}} + 1 - U_{\mathrm{v}})\frac{\partial\tilde{U}_{\mathrm{e}}}{\partial x}. \tag{15}$$

The solution for a plane wall with a small bump may easily be obtained by using the Prandtl transposition theorem (Rosenhead 1963) with $\hat{y} = y - H(\bar{x})$; the equations are the same in form as (4) with $v$ replaced by $v - u\,\mathrm{d}H/\mathrm{d}\bar{x}$; the only substantial difference is that the displacement thickness is given by

$$(u_{\mathrm{e}}\delta^*)_{\mathrm{hump}} = U_{\mathrm{e}}(\bar{x}, t)\, H(\bar{x}) + \int_0^\infty (U_{\mathrm{e}} - u)\,\mathrm{d}y. \tag{16}$$

Note that since $H = H(\bar{x}) = H(x + x_{\mathrm{v}}(t))$ the hump is moving in the coordinate system convecting with the vortex.

The present problem is complicated by the fact that the edge velocity is a function

of the displacement thickness, which itself is a function of the velocity. In other words, the pressure gradient in the interacting boundary layer is not known until the velocity at the edge of the boundary layer is found and vice versa, which is the novel feature of interacting-boundary-layer theory. Also $U_v$, the velocity at the vortex position, can only be found by considering the outer potential flow, and this is discussed in the next subsection.

### 2.2. *The potential flow*

It is well known that the inviscid flow due to a vortex in a uniform stream is given by

$$\left.\begin{aligned} U &= 1+\frac{k}{2\pi}\left\{\frac{Y+y_v}{(X-x_v)^2+(Y+y_v)^2}-\frac{Y-y_v}{(X-x_v)^2+(Y-y_v)^2}\right\}, \\ V &= \frac{k}{2\pi}\left\{\frac{X-x_v}{(X-x_v)^2+(Y-y_v)^2}-\frac{X-x_v}{(X-x_v)^2+(Y+y_v)^2}\right\}, \end{aligned}\right\} \tag{17}$$

where $(X, Y)$ are the (unscaled) inviscid flow coordinates non-dimensionalized with respect to $a$. The velocity components due to the displacement thickness are obtained by solving the problem for the potential, which is given by

$$\left.\begin{aligned} &\nabla^2\phi = 0, \\ &\frac{\partial\phi}{\partial Y} = \frac{\partial(U_e\delta^*)}{\partial X} \quad \text{on} \quad Y = 0, \\ &\phi \to 0, \quad X \to \pm\infty, \quad Y \to \infty. \end{aligned}\right\} \tag{18}$$

The solution to (18) is given in Van Dyke (1975, p. 49) and the results for the velocities are

$$\left.\begin{aligned} U_D &= \frac{Re^{-\frac{1}{2}}}{\pi}\int_{-\infty}^{\infty}\frac{(X-\xi)\,\partial(U_e\delta^*)/\partial\xi}{(X-\xi)^2+Y^2}\,d\xi, \\ V_D &= \frac{Re^{-\frac{1}{2}}}{\pi}\int_{-\infty}^{\infty}\frac{Y\,\partial(U_e\delta^*)/\partial\xi}{(X-\xi)^2+Y^2}\,d\xi. \end{aligned}\right\} \tag{19}$$

Consequently the total inviscid flow velocities are given by

$$u = U+U_D, \qquad v = V+V_D. \tag{20}$$

It should be noted that the vertical velocity at the edge of the boundary layer $V_e$ due to interaction can be written as (Burggraf 1982)

$$V_e = \frac{\partial(u_e\delta^*)}{\partial X}. \tag{21}$$

The vortex is advanced by evaluating (20) at $X = x_v$ and $Y = y_v$, and subtracting out the contribution due to the vortex itself; the equations are

$$U_v = \frac{dx_v}{dt} = 1+\frac{k}{4\pi y_v}+\frac{Re^{-\frac{1}{2}}}{\pi}\int_{-\infty}^{\infty}\frac{(x_v-\xi)\,V_e(\xi)}{(x_v-\xi)^2+y_v^2}\,d\xi, \tag{22}$$

$$V_v = \frac{dy_v}{dt} = \frac{Re^{-\frac{1}{2}}}{\pi}\int_{-\infty}^{\infty}\frac{y_v\,V_e(\xi)}{(x_v-\xi)^2+y_v^2}\,d\xi. \tag{23}$$

Note that $V_v = O(Re^{-\frac{1}{2}})$.

At this stage, we have formulated the problem for a plane wall and for a small hump and we can now discuss the numerical methods employed.

## 3. Numerical methods

The numerical scheme used in this study is a combination of finite-difference methods and the Fourier-transform method. First, in the $x$-direction, as mentioned previously, the Fourier-transform method is employed; in $y$, regular finite differences (with non-uniform grid) will be used. Finally, in $t$ the implicit Crank–Nicolson marching technique will be employed. To make the numerical scheme more efficient and also from physical considerations, coordinate transformations will be made in the $x$- and $y$-directions. This is based on the belief that most of the activity of the flow interaction is expected to occur around the vortex $x$-position and deep in the boundary layer. Hence by employing coordinate transformations, more grid points can be concentrated in the regions of intense activity near the boundary and the vortex $x$-position.

In deriving the difference equations for the numerical scheme, coordinate transformations are first applied to the original governing equation in $x$ and $\eta$ and, to this end, let

$$z = f(\eta), \qquad \xi = g(x). \tag{24}$$

Substituting these expressions into (12), the boundary-layer equation then becomes

$$4t\frac{\partial \tilde{u}}{\partial t} - f'^2\frac{\partial^2 \tilde{u}}{\partial z^2} - (f'' + 2\eta f')\frac{\partial \tilde{u}}{\partial z} = R(\xi, z, t), \tag{25}$$

where

$$R(\xi, z, t) = -4tg'\frac{\partial p}{\partial \xi} - 2t^{\frac{1}{2}}f'v\frac{\partial U_{\mathrm{R}}}{\partial z} - 4t(u_{\mathrm{R}} + \tilde{u} - U_{\mathrm{v}})g'\frac{\partial \tilde{u}}{\partial \xi} - 2t^{\frac{1}{2}}vf'\frac{\partial \tilde{u}}{\partial z},$$

where $f' = \mathrm{d}f/\mathrm{d}\eta$, $g' = \mathrm{d}g/\mathrm{d}x$. The tilde on $u$ in (25) will be dropped for convenience in the rest of the section. In the current study, the coordinate transformations used in $x-\xi$ and $\eta-z$ are

$$x = \sinh \tfrac{1}{3}\xi, \qquad \eta = \frac{2z}{1-z}. \tag{26}$$

The choice of sinh in this case satisfies the requirement of generating a fine grid around $x = 0$. The function in $z$ is similar to that used by Duck & Burggraf (1986) and resulted in a large decrease in the number of grid points required in the vertical direction. Taking the Fourier transform in the $\xi$-direction yields

$$4t\frac{\partial \bar{u}}{\partial t} - f'^2\frac{\partial \bar{u}}{\partial z^2} - (f'' + 2\eta f')\frac{\partial \bar{u}}{\partial z} = \bar{R}(\omega, z, t), \tag{27}$$

where an overbar is used to denote the Fourier transform of that quantity, which is defined as

$$\bar{F}(\omega) = \int_{-\infty}^{\infty} F(\xi)\,\mathrm{e}^{-\mathrm{i}\omega\xi}\,\mathrm{d}\xi. \tag{28}$$

The discretization of the Fourier transform is carried out as follows. Let

$$\left.\begin{aligned} \xi_j &= (j-1-m)\,\Delta\xi \quad \text{for } j = 1, 2, \ldots, N, \\ \omega_k &= (k-1-m)\,\Delta\omega \quad \text{for } k = 1, 2, \ldots, N, \end{aligned}\right\} \tag{29}$$

where $m$ is half the total number of grid points; i.e. $N = 2m$. The range of $\xi, \omega$ are chosen to ensure $F(\xi)$ and $\bar{F}(\omega)$ are small for $\xi < \xi_1, \xi > \xi_{N+1}$ and $\omega < \omega_1, \omega > \omega_{N+1}$ respectively. Since $F(\xi)$ is real, from (28) it can be shown that $\bar{F}(-\omega) = \bar{F}^*(\omega)$ where an asterisk denotes the complex conjugate of the quantity. The grid spacing $\Delta\xi$ and $\Delta\omega$ should now satisfy the relation

$$\Delta\xi\,\Delta\omega = \frac{2\pi}{N}, \tag{30}$$

and $N$ is required to be a power of 2 in the fast Fourier transform. The fast Fourier transform devised by Cooley & Tukey (1965) is used to evaluate the transformation.

To avoid the complicated convolution integral associated with the Fourier transform of the product of two quantities, the pseudospectral method will be used, i.e. all the nonlinear terms on the right-hand side of the governing equation will be evaluated in the physical domain using the predicted result of the previous iteration and then transformed to the spectral domain (Burggraf & Duck 1982). In this regard it is useful to discuss computation of terms involving differentiation with respect to $x$, say $u\,\partial u/\partial x$. Following Burggraf & Duck (1982), the velocity $u$ is computed by inverting the solution in transform space $\bar{u}$; to obtain $\partial u/\partial x$, the quantity $i\omega\bar{u}$ is inverted. The two terms are then multiplied together to obtain the required result in physical space; all other terms involving $\partial u/\partial x$ in $R$ are obtained in this way. It is to be noted that since the $x$-derivatives of $u$ are not numerically differentiated, there is no need for a special differencing procedure to incorporate the possibility of reversed flow. Indeed, this is the main advantage of computing the solution in transform space. As pointed out by Burggraf & Duck (1982), each point in physical space $x$ corresponds to a full range of points in spectral space; the possibility that regions of reversed flow may exist is automatically taken into account by the Fourier transform.

Equation (27) can be rewritten in compact form as

$$4t\frac{\partial\bar{u}}{\partial z} - f'^2\frac{\partial^2\bar{u}}{\partial z^2} - P\frac{\partial\bar{u}}{\partial z} = \bar{R}, \tag{31}$$

where $P = f'' + 2\eta f'$ and $\bar{R}$ is the right-hand side of (27). The finite-difference and the Crank–Nicolson techniques can then be applied in $z$ and $t$, which yields

$$4(t-\tfrac{1}{2}\Delta t)\frac{\bar{u}^t - \bar{u}^{t-\Delta t}}{\Delta t} - \tfrac{1}{2}f'^2\left(\frac{\partial^2\bar{u}^t}{\partial z^2} + \frac{\partial^2\bar{u}^{t-\Delta t}}{\partial z^2}\right) - \tfrac{1}{2}P\left(\frac{\partial\bar{u}^t}{\partial z} + \frac{\partial\bar{u}^{t-\Delta t}}{\partial z}\right) = \tfrac{1}{2}(\bar{R}^t + \bar{R}^{t-\Delta t}). \tag{32}$$

$\partial^2\bar{u}/\partial z^2$ and $\partial\bar{u}/\partial z$ are evaluated by using central differencing and $P$ is evaluated at $t-\frac{1}{2}\Delta t$. The equation can then be solved for $\bar{u}^t$ in terms of the values at the previous time-step; values of $\bar{u}^t$ for $\bar{u}$ at $t = 0$ are found by using the initial condition given by (14) and the values for $\bar{v}$ are then found by using the continuity equation. The truncation errors for the scheme are of order $(\Delta t)^2$ and $(\Delta z)^2$ because of the central differencing used here.

To complete the formulation of the numerical scheme, the boundary conditions, the interaction condition (6), the pressure gradient (15) and the vortex path equations (22), (23) also have to be considered. For finding the displacement thickness in (7), the Simpson $\frac{1}{3}$-rule is used. For the interacting boundary condition, (6), the finite-difference method similar to that used in Veldman (1981) is employed, in which the integral is approximated at the midpoint of each interval. From

Veldman (1981) for a general differentiable function $A$ the scheme can be written as

$$J_i = \int_{-\infty}^{\infty} \frac{A'}{x_i - \xi} \mathrm{d}\xi = h \sum_{j=0}^{N-1} \frac{A'_{j+\frac{1}{2}}}{x_i - x_j - \frac{1}{2}h}, \tag{33}$$

where $h$ is the grid size in the $\xi$-direction. The value of (33) is its simplicity; however, as pointed out by Napolitano, Werle & Davis (1978) (the existence of which was brought to our attention by Professor J. D. A. Walker), this scheme yields only first-order-accurate results.

Thus, at lower Reynolds numbers, where the interaction between the boundary layer and the inviscid flow is expected to be stronger, puzzling results were obtained using (33). For example, for $Re = 44000$ the calculation breaks down at about $t = 0.94$, and for $Re = 8000$, the calculation is abruptly terminated at $t = 0.81$ before the interaction regime was reached. Consequently, a new second-order formula, originally devised by Napolitano *et al.* (1978), was applied to the present problem. The method is described as follows: here $\bar{x}_i = x_i + \frac{1}{2}\Delta x_i$, and

$$I(\bar{x}_i) = \int_a^b \frac{s(t)}{\bar{x}_i - t} \mathrm{d}t = \sum_{j=1}^{N-1} \int_{x_j}^{x_{j+1}} \frac{s(t)}{\bar{x}_i - t} \mathrm{d}t. \tag{34}$$

Using a Taylor series approximation we evaluate $s(t)$ at the midpoint of the interval $\bar{x}_j$; then

$$\begin{aligned} I(\bar{x}_j) &= \sum_{j=1}^{N-1} \left[ s(\bar{x}_j) \int_{x_j}^{x_{j+1}} \frac{1}{\bar{x}_i - t} \mathrm{d}t + \sum_{j=1}^{N-1} \frac{\partial s}{\partial t}\bigg|_{x_j} \int_{x_j}^{x_{j+1}} \frac{t - \bar{x}_j}{\bar{x}_i - t} \mathrm{d}t \right] \\ &= \sum_{j=1}^{N-1} \left[ \frac{(s_{j+1} + s_j)}{4} \log\left( \frac{\bar{x}_j - x_j}{\bar{x}_i - x_{j+1}} \right)^2 \right. \\ &\quad \left. + \frac{s_{j+1} - s_j}{x_{j+1} - x_j} \left[ \frac{\bar{x}_i - \bar{x}_j}{2} \log\left( \frac{\bar{x}_i - x_j}{\bar{x}_i - x_{j+1}} \right)^2 - x_j \right] \right], \end{aligned} \tag{35}$$

to second order, where $\Delta x_j = x_{j+1} - x_j$. Here we apply (34) for $s = \partial(U_e \delta^*)/\partial x$ and we use second-order central differencing on the variable $x$-grid to do this; we have also differenced in the $\xi$-plane using the relationship between $x$ and $\xi$ with no change in the results. It should be noted that the Cauchy integral $I$ is evaluated at $\bar{x}_j$ and to obtain its value at the regular grid points $x_j$, standard second-order Lagrangian interpolation was used. Smith & Bodonyi (1985) and Riley (1982) have developed similar, higher-order schemes to evaluate the Hilbert integral.

It should be noted here that the edge condition $u = U_e$ at $\eta \to \infty$ is satisfied iteratively at each time-step. This was done to enable a non-uniform grid spacing in the streamwise direction $x$ to be used; smaller physical grid sizes are necessary in order to resolve the fine structure of the flow near $x = 0-$. The alternative is to use a constant streamwise grid spacing with the edge condition $u = U_e$ satisfied in spectral space directly at each time-step. However, at least twice as many grid points would be required in the streamwise direction to satisfy the accuracy requirements, which are severe in the latter stages of the calculations, and it is unlikely that this procedure would yield results significantly different from the present results, for the times and Reynolds numbers considered here.

The pressure gradient, (15), is calculated by using central differencing in $t$ and central differencing in $\xi$. For the initial time-step, two-point backward differencing is used. Also the boundary condition in the $y$-direction is imposed at some large but finite value of $\eta$, say $\eta = l$, as an approximation (see below).

The iteration scheme used in this study is summarized as follows. The scheme consists of two main loops. Within the inner loop, the boundary-layer equations are solved for a specific time-step iteratively. The procedure is as follows. First, (32) can be written in tridiagonal form and is solved by using the Thomas algorithm to obtain values of velocity $\bar{u}$ at all points of the spectral domain. By inverting $\bar{u}$ back to the physical domain, the displacement thickness $U_e\delta^*$ can then be calculated. The subroutine for the interacting boundary condition ((5*a*) with (33)) is then called on to obtain the edge velocity $U_e$ of the boundary layer. The pressure gradient is next computed by using the Euler equation, (15). The vortex is then advanced by (22) and (23) using a central differencing scheme in time $t$. The process is repeated until the change of $\bar{u}$ in successive iterations is less than a specified absolute tolerance value, in this case, $10^{-4}$ or $10^{-5}$. The calculation then continues to the outer loop where time marching is performed. In solving (32) for $\bar{u}$, under-relaxation was used according to the formula

$$\bar{u} = \omega_r \bar{u}_{new} + (1-\omega_r)\bar{u}_{old}, \tag{36}$$

where $\omega_r$ is the relaxation factor. Various values of $\omega_r$ have been used for different cases to ensure the convergence of the numerical scheme. In most cases, $\omega_r = 0.4, 0.3,$ or 0.2 were used. The number of iterations in each time-step is generally around 10–15 at the early stages. At increasing times and with intense variation in the flow field, 20–30 iterations were required to achieve a convergent solution. At lower Reynolds numbers up to 50 iterations were required for a tolerance of $10^{-5}$ and $\omega_r = 0.2$.

The accuracy of the scheme was first checked by running the program for the non-interacting cases corresponding to those of Doligalski & Walker (1984). It was found that agreement between the streamline patterns at different time-steps was good. A detailed discussion of this aspect of the calculation will be presented in §4. The scheme was further tested for different grid sizes in $\xi$, $z$ and $t$. The agreement between different grid sizes and time-steps was very good especially for large values of $\alpha$. In the $z$-direction, based on these tests, 33 points across the boundary layer were employed; 128 points were used in the $x$-direction. The boundary conditions at $\xi = \pm\infty, \eta = l$ were also checked. In the numerical scheme, finite values are employed to approximate these infinite values. And the results showed that $\eta = l = 6$ is generally adequate for the maximum value for most of the cases, although in some cases larger values had to be used in the later stages of the calculation because of the growth of the boundary layer with time. For the boundary conditions in $\xi$, a sufficient range has to be chosen to ensure that the disturbance velocity beyond that is small and negligible. Tests for different ranges showed that $-11.2 \leqslant \xi \leqslant 11.0$, which in the $x$-domain corresponds to $-19 \leqslant x \leqslant 19$, is adequate to ensure five significant figure agreement in the results with the results of larger ranges. A typical time-stepping employed in this work was $\Delta t = 0.001$ for the first 25 time-steps, then $\Delta t = 0.025$ for the majority of the rest of the calculations. In many cases the time-step was further reduced near breakdown of the numerical scheme; for $\alpha = 0.2$, $\Delta t = 0.01563$ was used 10 steps before failure and in §5 $\Delta t = 0.010$ was used after time-step 57, $\Delta t = 0.005$ after time-step 66.

The numerical method used in this study is believed to be superior to that of Doligalski & Walker (1984). Approximately half the number of grid points were employed for the current method to achieve similar results: generally the maximum number of mesh points used in this study is about 10000 while in Doligalski & Walker (1984), a maximum of 22000 points were required at times near failure of the numerical scheme. This reduction in the number of grid points can be attributed to

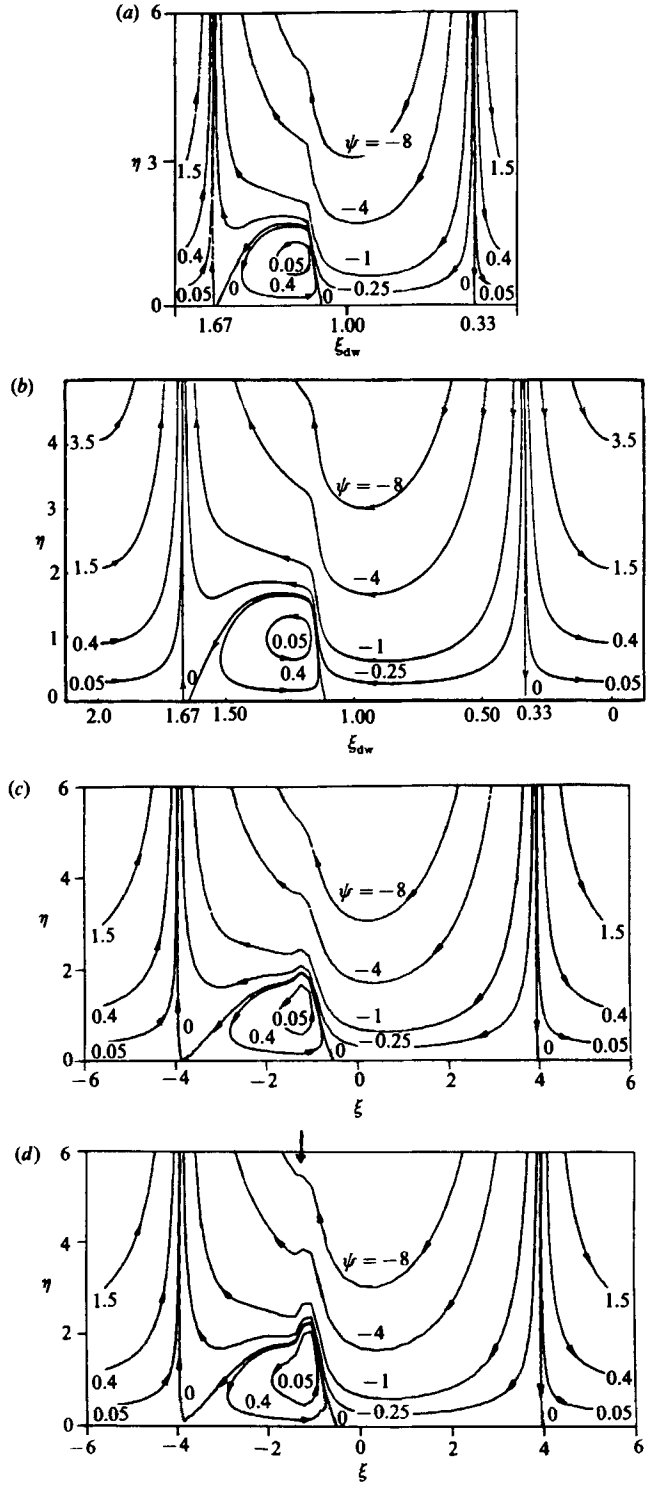


FIGURE 2. Streamlines relative to the vortex for $\alpha = 0$: (*a*) present results, non-interacting, $t = 0.65$; (*b*) Doligalski & Walker (1984) results, $t = 0.65$; (*c*) interacting, $t = 0.65$, $Re = 8 \times 10^{-4}$; (*d*) interacting, $t = 0.70$, $Re = 8 \times 10^{4}$. Labels correspond to constant $\psi$.

the use of non-uniform grids in $x$ and $y$ and also to the FFT method in $x$ as discussed earlier. However, the results in the next section indicate that for the non-interacting case the current method cannot go further in time despite the use of an FFT method.

## 4. Results for $Re = 8 \times 10^4$

### 4.1. *The plane wall results*

Solutions have been computed for a variety of vortex strengths and to check the validity of the program; non-interacting solutions for the plane wall have been computed for the vortex strengths considered by Doligalski & Walker (1984); $Re = 8 \times 10^4$ has been chosen for comparison with that work. The general features of the solutions as a function of $\alpha$ have been reproduced; that is, for $\alpha < 0.55$ a separation bubble forms deep within the boundary layer and grows with time, eventually forcing the breakdown of the numerical scheme. Typical results for the streamline patterns are shown on figure 2(*a*); the stream function $\psi$ is defined in the usual way:

$$u = \frac{\partial \psi}{\partial y}, \quad v = -\frac{\partial \psi}{\partial x},$$

and the streamline patterns are relative to the vortex unless otherwise noted. For ease of comparison with Doligalski & Walker (1984), our solutions have been plotted on the same $x$-scale as their solution for infinite Reynolds number, which appears on figure 2(*b*). This comparison is for $\alpha = 0$ at $t = 0.65$ and other cases produced comparable results. Note that the two solutions are almost identical and consequently our solution appears to reduce correctly when interaction is absent.

The effect of interaction is exhibited by comparison of figure 2(*c*) with 2(*a*) or 2(*b*). Figure 2(*c*) is the interacting solution at $t = 0.65$ for $Re = 8 \times 10^4$; note that the streamwise scale on this figure is different from figures 2(*a*) and 2(*b*). Nevertheless the effect of interaction can be seen to modify the shape of the eddy near its top. On figure 2(*d*) is the solution for $t = 0.70$, just before breakdown of the solution. Note that a streamwise interacting scale appears to be emerging and this is denoted by the arrow on figure 2(*d*); it is this scale that will be compared with the streamwise scale deduced by Elliott *et al.* (1983).

On figures 3 and 4 are a sequence of patterns at different times with figure 3 being the non-interacting sequence and figure 4 the interacting sequence for $\alpha = 0.2$; the interacting sequence is for $Re = 8 \times 10^4$. Note that the effect of interaction is fairly weak until the later times and that the kinking of the streamline patterns is clearly evident in the non-interacting patterns at $t = 0.88$. The effect of interaction here is to round off the top of the eddy, which allows the calculation to proceed further. The interacting case breaks down shortly after $t = 0.94$. Note the emergence of a small side lobe which appears to be the beginning of a tertiary eddy; this side lobe was not present in some of the coarser-time-stepping calculations (figure 4*d* has $\Delta t = 0.005$ at $t = 0.94$). Again the streamwise interaction scale appears to emerge only after the non-interacting program has failed (which is really only valid at infinite Reynolds number anyway) and the scale is about the same width as for $\alpha = 0$. Similar results are obtained for $\alpha = 0.4$, the interacting case of which is presented on figure 5 for two times; it should be noted that the interaction scale (i.e. the shear layer) appears to be independent of $\alpha$.

The effect of interaction allows the computation to proceed further in time; the growth of the eddy apparently forces the vortex further out into the free stream, as

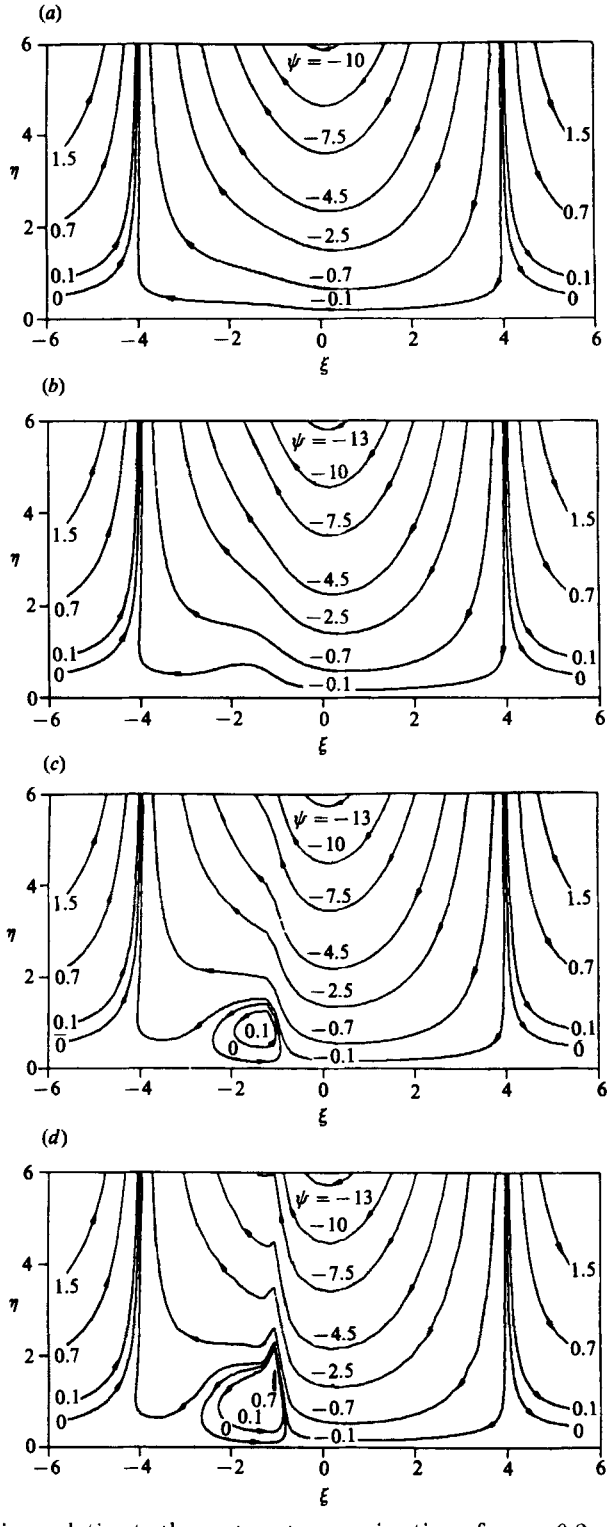


FIGURE 3. Streamlines relative to the vortex at successive times for $\alpha = 0.2$; non-interacting. These are the Doligalski & Walker (1984) solutions computed with our code: (*a*) $t = 0.25$, (*b*) $t = 0.5$, (*c*) $t = 0.75$, (*d*) $t = 0.88$. Labels correspond to constant $\psi$.

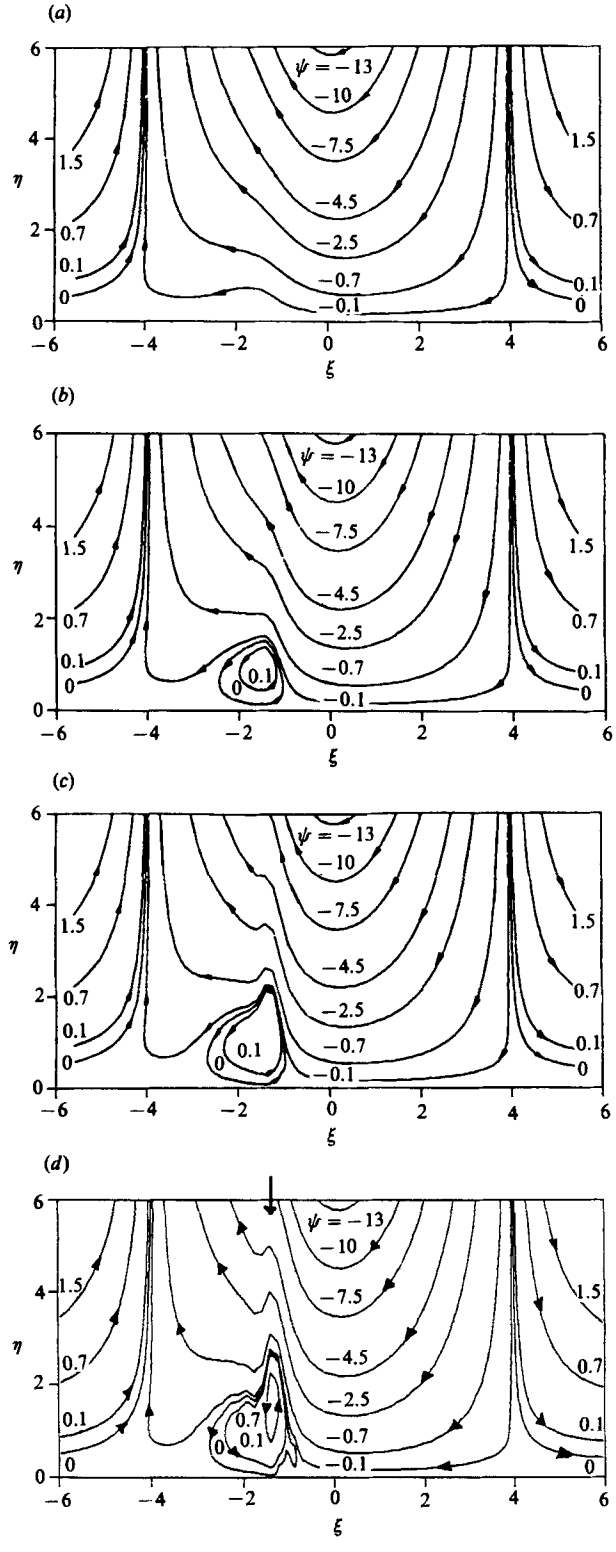


FIGURE 4. Streamlines relative to the vortex at successive times for $\alpha = 0.2$; interacting: (*a*) $t = 0.5$, (*b*) $t = 0.75$, (*c*) $t = 0.88$, (*d*) $t = 0.94$; $Re = 8 \times 10^4$. Labels correspond to constant $\psi$.

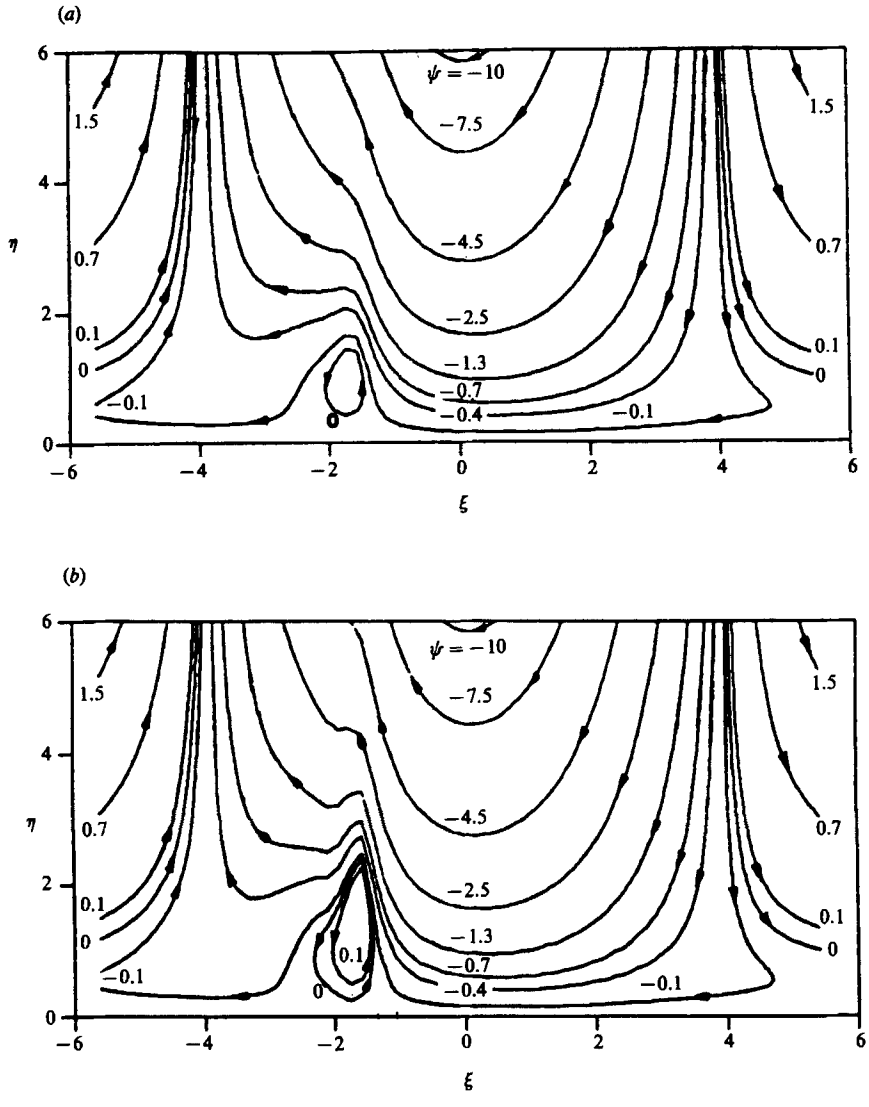


FIGURE 5. Streamline patterns relative to the vortex for $\alpha = 0.4$; (*a*) $t = 1.08$, (*b*) $t = 1.25$; $Re = 8 \times 10^4$. Labels correspond to constant $\psi$.

shown in figure 6 where the position of the vortex is plotted. The fact that the vortex gets pushed further into the outer flow allows further growth of the eddy and the computation proceeds further in time.

One additional comment may be made concerning the solutions presented; the displacement thickness results are not significantly altered by the effect of interaction for $\alpha < 0.55$; this is apparently because the integrand defining $\delta^*$, $1 - u/U_e$ remains approximately the same as in the non-interacting case; in ay event, no significant differences in the displacement thickness were observed for $\alpha < 0.55$. It is interesting to note here, however, that for $\alpha = 0.8$ there was a significant change. At about this vortex speed the vortex is actually driven down into the boundary layer slightly and this apparently causes an increase in displacement thickness directly under the

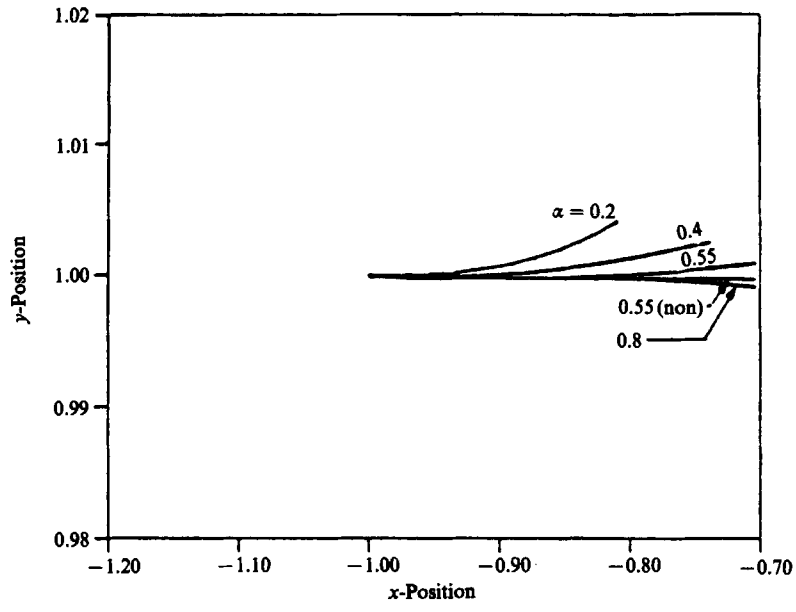


FIGURE 6. Vortex path for different $\alpha$-values in the interacting cases (labels correspond to $\alpha$).

vortex. On figure 7 is depicted the displacement thickness for both the interacting and non-interacting cases; note that $\delta^*$ is actually smaller behind the vortex for the interacting case but larger directly under the vortex.

Similar results were obtained for the case of a hump within the boundary layer and these results are discussed next.

### 4.2. *Solutions for a hump*

To deduce the effect of an irregular surface shape, solutions have also been produced for a hump of the form

$$\begin{aligned} H(\bar{x}) &= \beta(1-\bar{x}^2)^2 \quad \text{for } |\bar{x}| \leqslant 1 \\ &= 0 \qquad\qquad\quad \text{for } |\bar{x}| \geqslant 1. \end{aligned} \tag{37}$$

We have produced solutions for $\beta = 5.0$ and will consider the results for $\alpha = 0$, 0.2, and 0.55 for $Re = 8 \times 10^4$. It should be noted here that in a coordinate system moving with the vortex, the hump moves to the left as time $t$ increases since $H = H(\bar{x})$; hence $H$ is also a function of time $t$. In general, the hump destabilizes the calculation somewhat in the sense that it hastens breakdown. The results are shown on figure 8(*a–c*); the temporal development is similar to that without the hump. Figure 8(*a*) shows the solution for $\alpha = 0$ at $t = 0.55$; note that the eddy is located on the leeward side of the hump; the position of the hump is slightly off-centre because the plots are in terms of $\eta = y/2t^{\frac{1}{2}}$. On figure 8(*b*) is the solution for $\alpha = 0.2$ at $t = 0.75$; note that the eddy is somewhat shorter than for $\alpha = 0$; the eddy moves to the windward side of the hump for $\alpha = 0.55$, which is shown on figure 8(*c*) at $t = 1.78$ and is thinner than for the smaller $\alpha$. The streamwise interaction scale in this case is also clearly seen in figure 8(*c*) and is about the same width as in the previous no-hump cases.

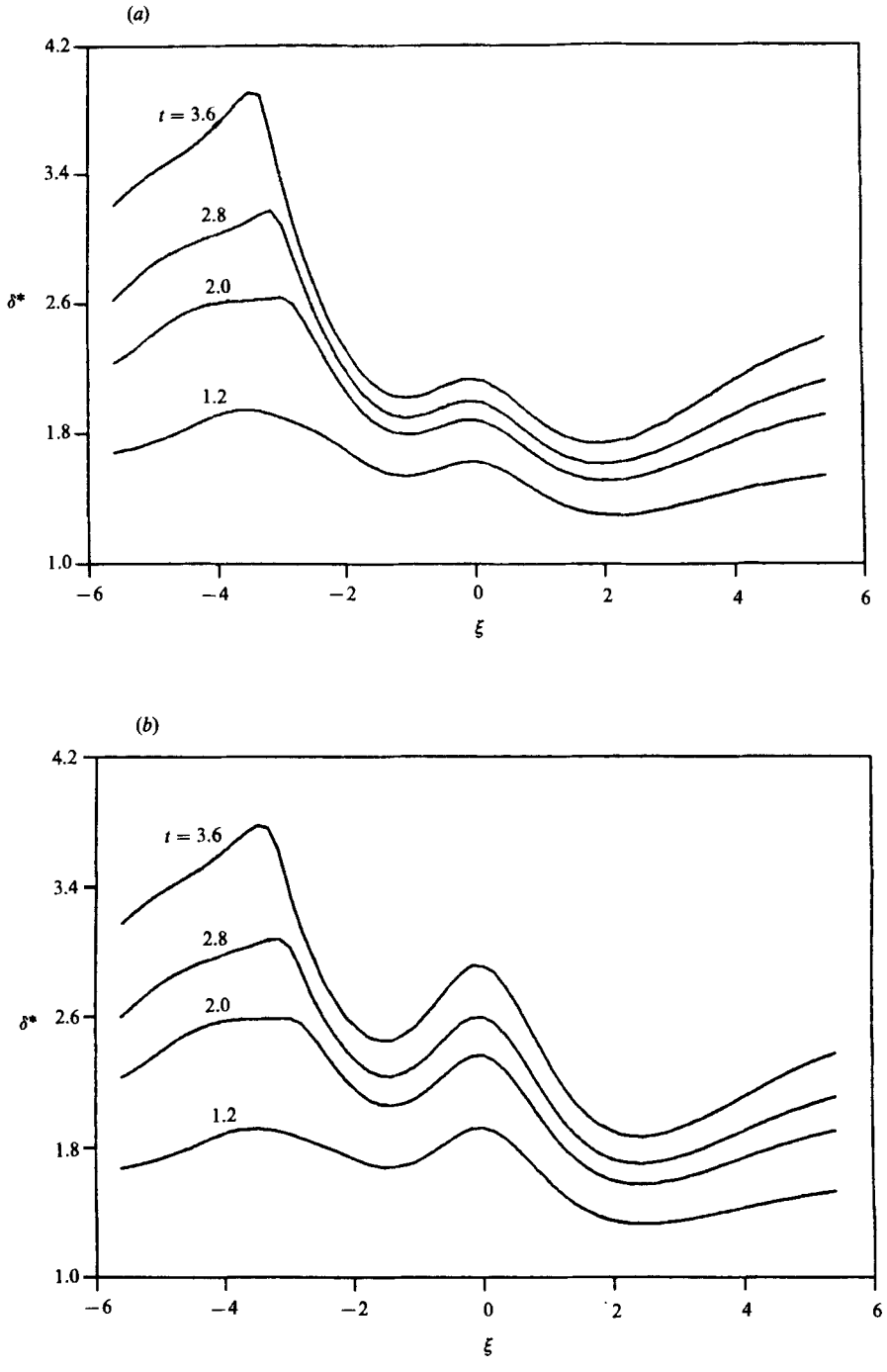


FIGURE 7. Displacement thickness for $\alpha = 0.8$. (*a*) non-interacting, present code; (*b*) interacting, $Re = 8 \times 10^4$. Labels correspond to different times and plot is in the laboratory frame, not relative to the vortex.

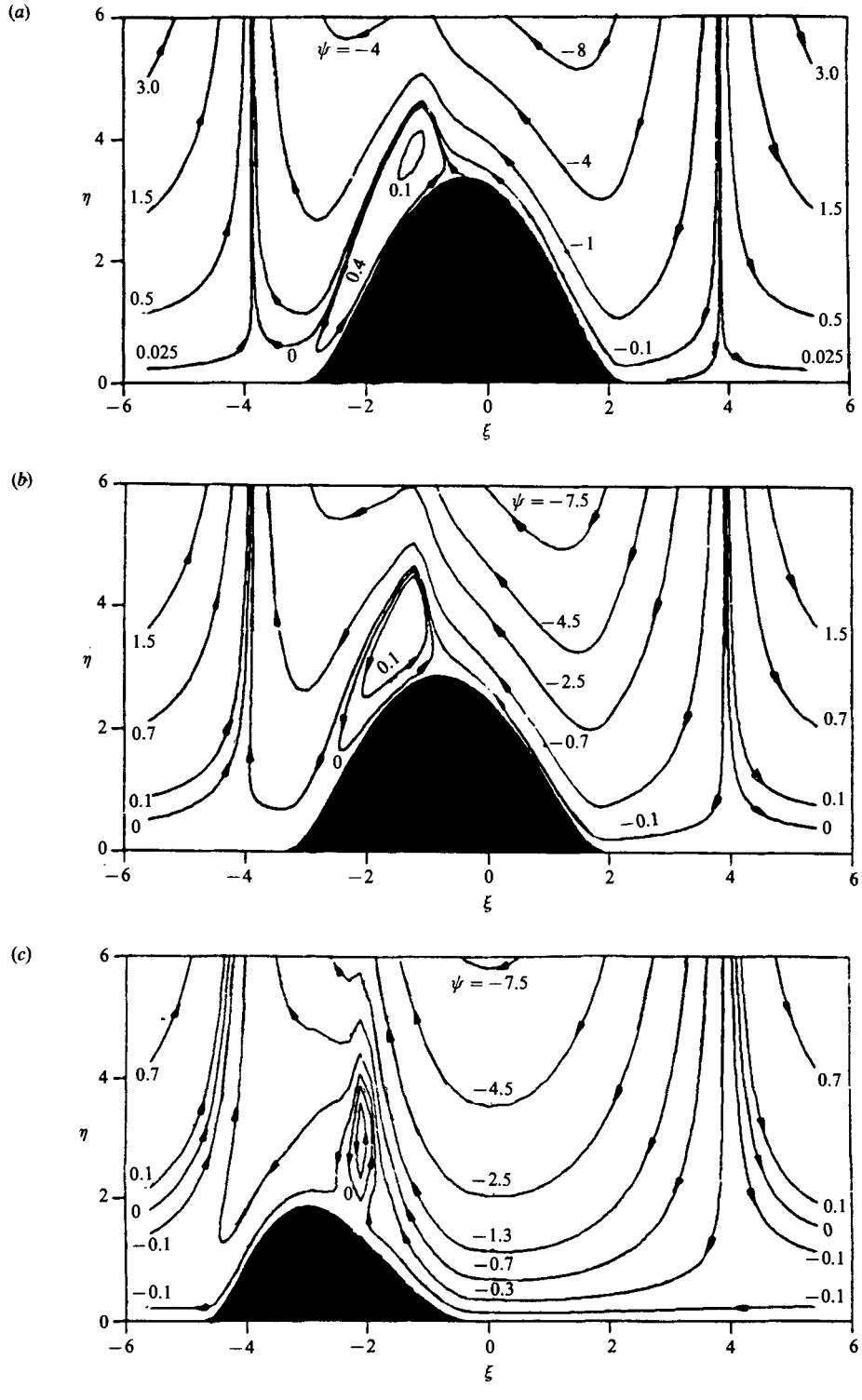


FIGURE 8. Streamline patterns relative to the vortex for a plane wall with a hump with $\beta = 5$, $Re = 8 \times 10^4$, interacting: (*a*) $\alpha = 0$, $t = 0.55$; (*b*) $\alpha = 0.2$, $t = 0.75$; (*c*) $\alpha = 0.55$, $t = 1.78$. Labels correspond to constant $\psi$.

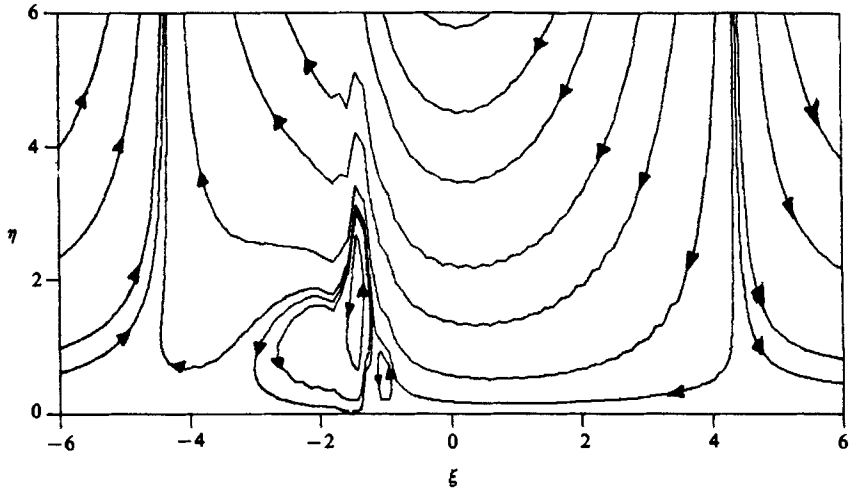


FIGURE 9. Streamline patterns for $Re = 8 \times 10^4$ at $t = 0.94$ using the Napolitano *et al.* (1978) scheme. The streamline values are the same as in figure 4.

## 5. The effect of Reynolds number

It has been established that the basic eruption mechanism is the same for all $\alpha < 0.55$, and in this section results will be presented for $\alpha = 0.2$. The calculations for $Re = 8 \times 10^4$ using the Napolitano *et al.* (1978) scheme appear to agree with those using the Veldman scheme for times $t \leqslant 0.88$ which, for $\alpha = 0.2$, is somewhat within the interactive phase of the motion. However, at smaller Reynolds numbers, use of the more accurate Cauchy integrator is crucial to obtain results well into the interactive regime. As mentioned previously, the calculations at the lower Reynolds numbers would mysteriously break down before the interactive regime was reached.

Additional grid and time-step studies were performed and it was found that 33 points in the $x$-direction were sufficient as with the Veldman scheme; however, with the Napolitano *et al.* scheme, it was found that a smaller $\xi$-grid improved the results significantly, especially at the larger times and lower Reynolds numbers of interest in this section.

It should be mentioned that ideally a small $\Delta\omega$ as well as small $\Delta\xi$ is necessary for an accurate solution; that is, the solution needs to be accurate in spectral space as well as in physical space. This fact is illustrated in the relationship $\Delta\omega = 2\pi/N\Delta\xi$; note that as $\Delta\xi$ is decreased, $\Delta\omega$ is increased and since the error in approximating the Fourier integral is $O(\Delta\omega)^2$ the error in the spectral plane actually increases as $\Delta\xi$ decreases. The accuracy problem is aggravated for times $t \gtrsim 0.92$ (for $\alpha = 0.2$) where the effect of interaction is greatest. The effect of increasing $\Delta\omega$ emerges in aliasing within the spectral solution at the ends of the spectral grid, which affects the solution near $\xi = 0$ in the physical grid. As mentioned previously, for times less than about 0.88 (for $\alpha = 0.2$), for all Reynolds numbers tested, a physical grid size of $\Delta\omega = 0.175$ with $N = 128$ was suitably accurate when comparing streamline patterns and vertical velocities at the edge of the boundary layer. However, for times greater than about 0.88, it was found that a smaller $\xi$-grid was required with $\Delta\xi = 0.12, N = 256$. Smaller $\Delta\xi$ resulted in increased aliasing in the spectral grid and the results for $\Delta\xi = 0.14$ are not significantly different from those of $\Delta\xi = 0.12$. Nevertheless, because obtaining solutions in the strongly interactive phase of the motion is so

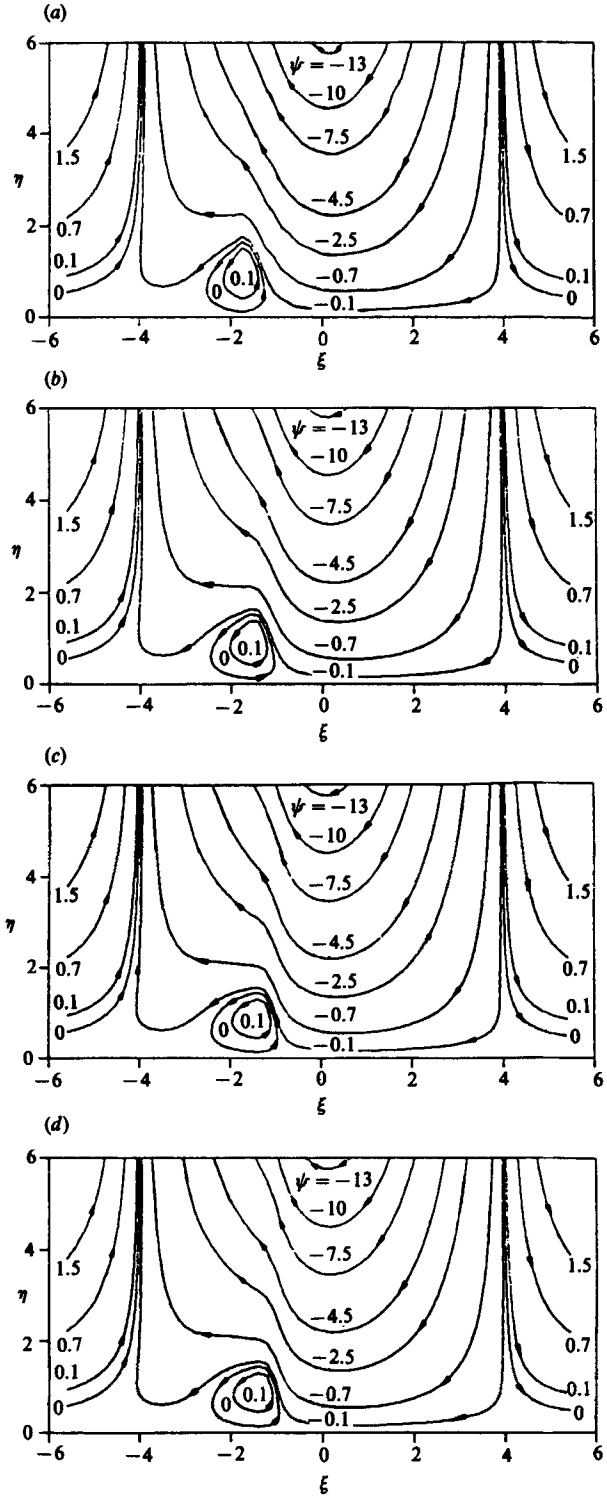


FIGURE 10. Streamlines relative to the vortex at $t = 0.75$ for several Reynolds numbers; here $\alpha = 0.2$ and the solutions are for the interacting case: (*a*) $Re = 8 \times 10^3$, (*b*) $Re = 4.4 \times 10^4$, (*c*) $Re = 4.4 \times 10^5$, (*d*) $Re = 8 \times 10^5$. Labels correspond to constant $\psi$.

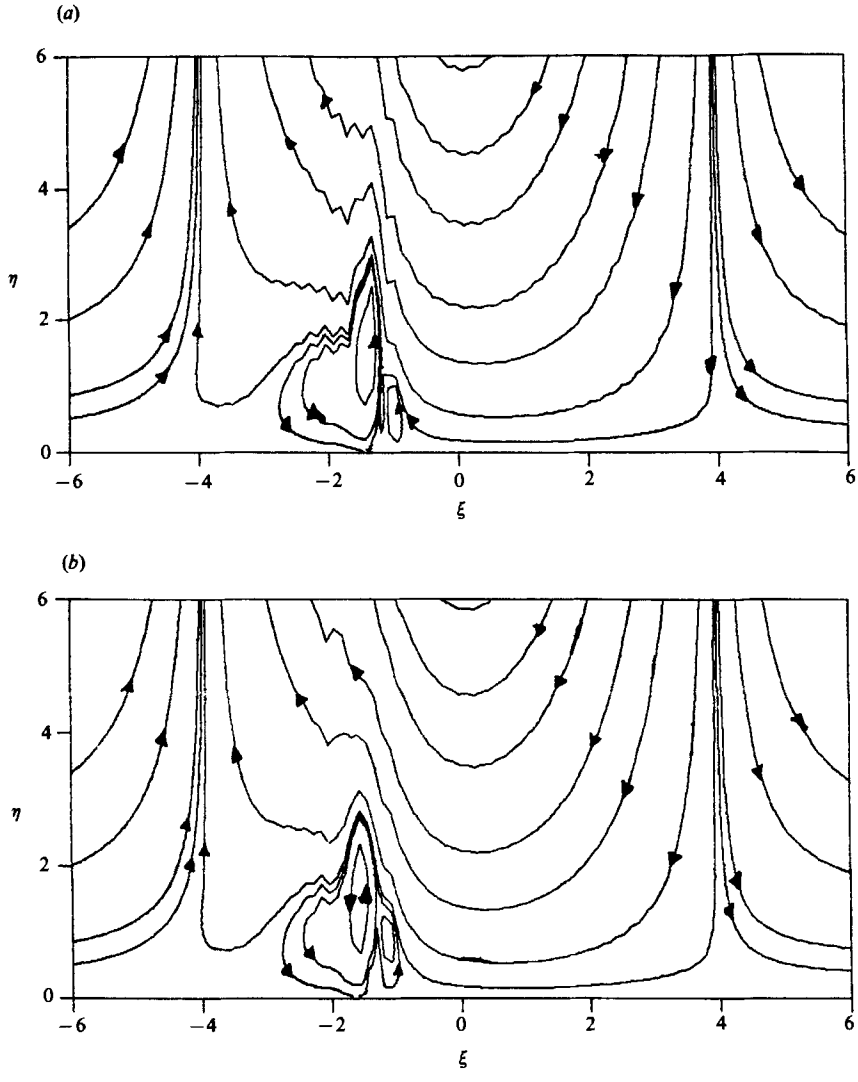


FIGURE 11. Streamline patterns at $t = 0.94$ for two Reynolds numbers. (*a*) $Re = 4.4 \times 10^4$, (*b*) $Re = 2.2 \times 10^4$. Streamline values are the same as in figure 4.

crucial, the results of this section are for $\Delta\xi = 0.12, N = 256$. This corresponds to a grid size in the $x$-plane of about 0.04 near the formation of the secondary eddy. Additional runs were made with $N = 512$ and a constant grid size of $\Delta x = 0.04$ with a slight improvement in aliasing (i.e. somewhat smaller 'wiggles'); however the streamline patterns and the vertical velocity at the edge of the boundary layer are substantially unchanged. A smaller time-step has been used in the results of the present section and here $\Delta t = 0.005$ or 0.0025 in the latter stages of the calculations.

On figure 9 are the streamline patterns for $Re = 8 \times 10^4$ at $t = 0.94$ calculated using the new scheme. Note the presence of a tertiary eddy with the same rotation as the main eddy at about $\xi = -1$; such an eddy has been observed in the experimental work of Walker *et al.* (1987) and more will be said about this subsequently.

Figure 10 shows results computed for various Reynolds numbers at $t = 0.75$ before

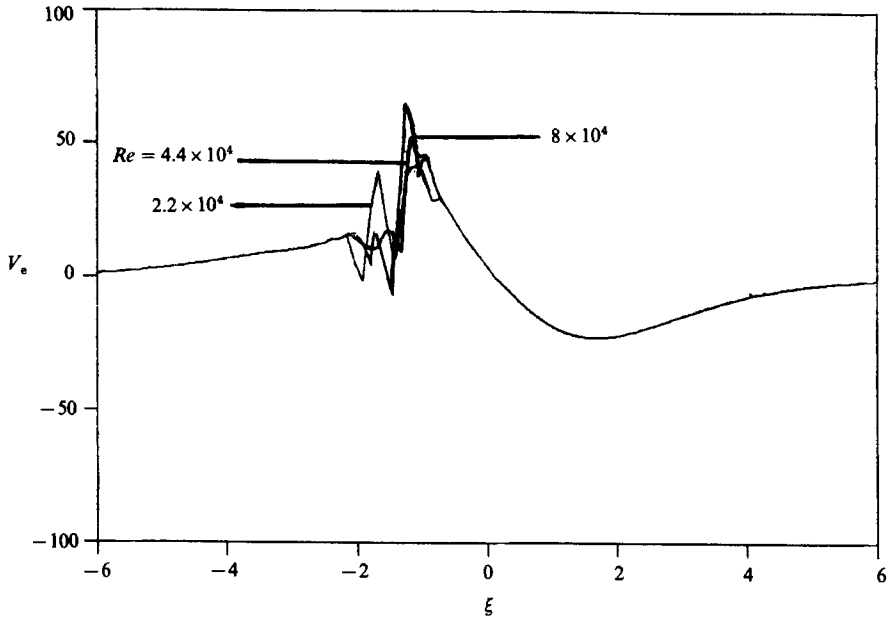


FIGURE 12. Vertical velocity at the edge of the boundary layer at $t = 0.94$ for several Reynolds numbers.

the strong interaction regime is reached. Note that at this time, very little difference is observed in these streamline patterns for different Reynolds numbers.

Figure 11 is a sequence of results for two other Reynolds numbers at $t = 0.94$ to illustrate the structure of the interaction regime. Note that as the Reynolds number decreases, the interaction appears weaker at this (fixed) time as the vortex gets pushed further into the outer flow. Note also that the interaction region gets wider as $Re$ decreases. The vertical velocity at the edge of the boundary layer is shown on figure 12 for the cases of figure 11 and for $Re = 80000$. The time $t = 0.94$ is close to the time at which the numerical scheme breaks down for $Re = 80000$ and so the amplitude of the edge velocity is very large. As the Reynolds number decreases, the amplitude reduces since the interaction prolongs the calculation.

To illustrate the temporal development of the flow, on figure 13 are depicted results for $Re = 44000$ for times $t = 0.88, 0.90, 0.92, 0.96$. This sequence of figures is presented to illustrate the development of the tertiary eddy from a small side lobe which begins to form at about $t = 0.88$. By $t = 0.92$ the lobe is about ready to break off and by $t = 0.96$ the solution has begun to develop a numerical instability (i.e. the wiggles) near the shear layer position which appears to be a result of aliasing in the spectral grid. By $t = 0.98$ (not shown) the numerical instability has spread and the results are no longer very accurate although the calculations may be continued a short time further. On figure 14 are the results for the edge velocity at $t = 0.88, 0.92, 0.96$, for $Re = 44000$. It should be noted that the sharp spikes depicted on figures 12 and 14 in the edge velocity appear to be physical and are present for all grid sizes tested (see for example, Henkes & Veldman 1987, figures 5, 6).

The presence of a tertiary eddy on figures 9, 11, 13 is especially interesting. As mentioned previously, Walker *et al.* (1987) have investigated the interaction of a vortex ring with a boundary layer and in flow visualization studies have observed the

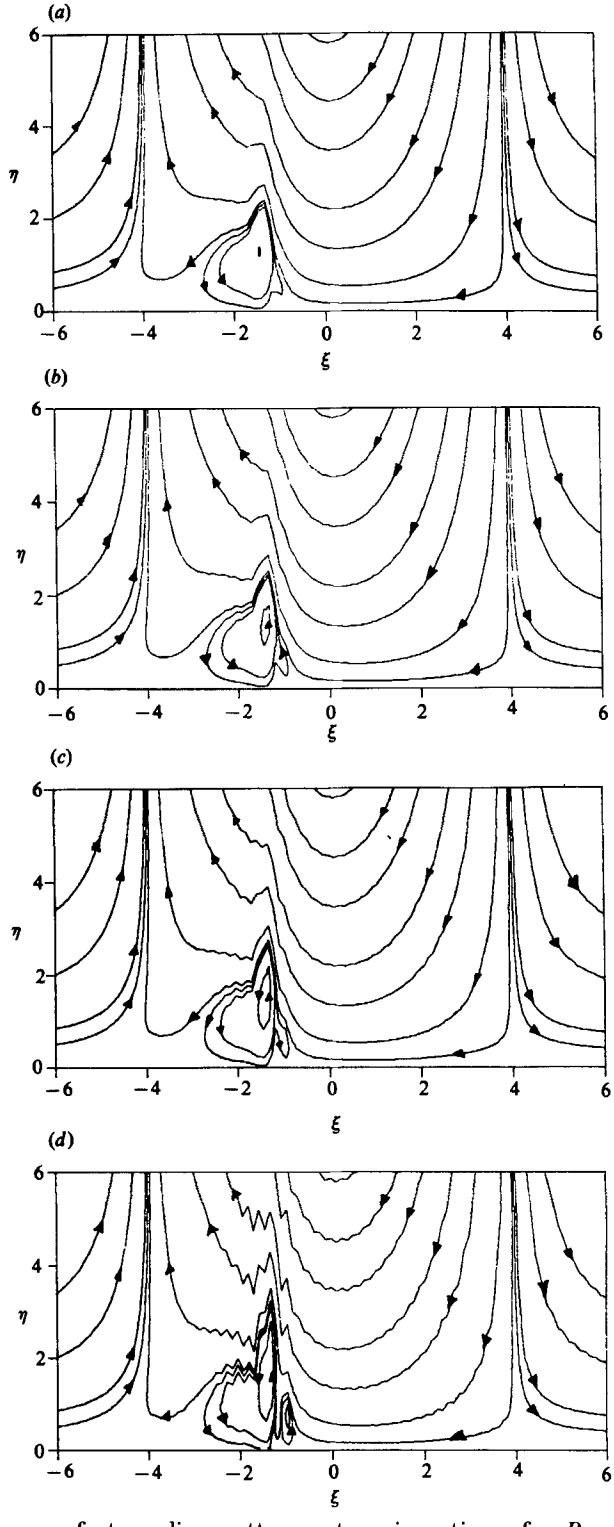


FIGURE 13. Sequence of streamline patterns at various times for $Re = 4.4 \times 10^4$ illustrating development of tertiary eddy. (*a*) $t = 0.88$, (*b*) $t = 0.90$, (*c*) $t = 0.92$, (*d*) $t = 0.96$. See figure 11 (*a*) for the results at $t = 0.94$.

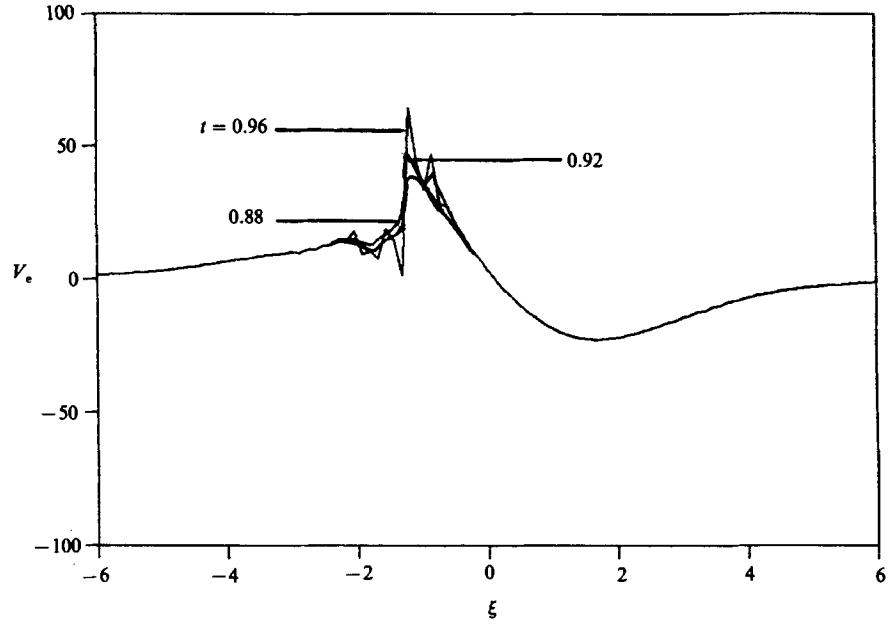


FIGURE 14. Vertical velocity at the edge of the boundary layer for $Re = 4.4 \times 10^4$ for several times corresponding to results depicted on figure 13.

(*a*)

| *Re* | *x* | *y* |
|---|---|---|
| 80000 | −0.81511 | 1.00379 |
| 44000 | −0.81618 | 1.00512 |
| 22000 | −0.81786 | 1.00723 |

(*b*)

| *t* | *x* | *y* |
|---|---|---|
| 0.88 | −0.82787 | 1.00426 |
| 0.90 | −0.82397 | 1.00454 |
| 0.92 | −0.82007 | 1.00482 |
| 0.96 | −0.81228 | 1.00543 |

TABLE 1. (*a*) Vortex position at $t = 0.94$ for several Reynolds numbers. The initial position of the vortex is $(-1, 1)$. (*b*) Vortex position at various times for $Re = 44000$.

formation of a tertiary vortex outboard of the primary vortex ring and of the same signed vorticity as the secondary ring (see figures 8 and 9 of Walker *et al.* 1987). Although the ring problem is three-dimensional and the three vortices are not in the same relative positions as in the present work, the formation of a tertiary eddy appears consistent with the experimental results of that paper. The formation of this third eddy has occurred for all Reynolds numbers, $Re \lesssim 80000$ where interaction processes are significant and cannot be predicted by classical boundary-layer theory.

The vortex path variation as a function of Reynolds number using the Napolitano *et al.* scheme is similar to that depicted on figure 9 for different values of $\alpha$; to

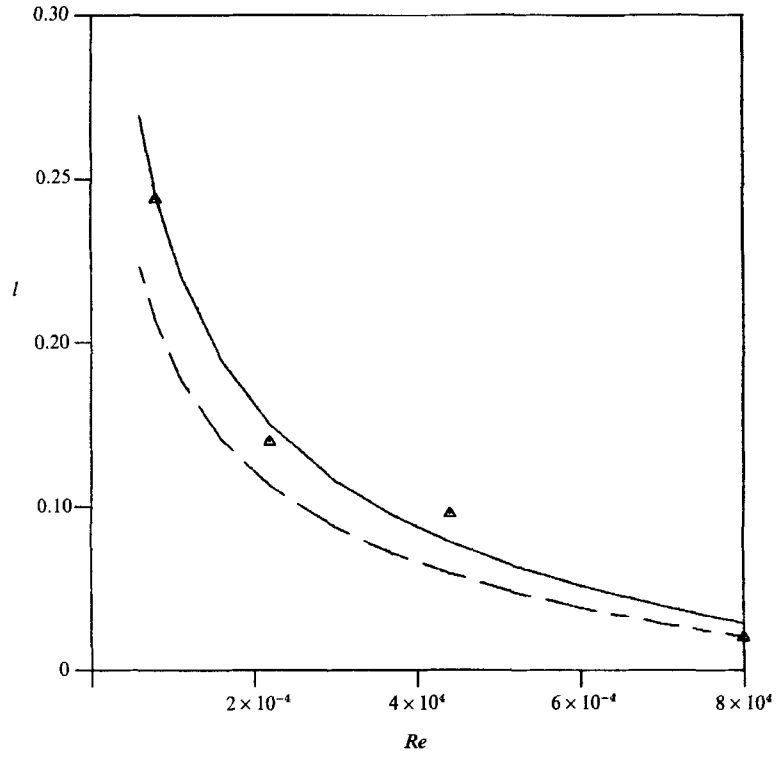


FIGURE 15. Width of the interaction region $l$ as a function of Reynolds number $Re$; the solid line is a least-squares fit $l = 4.796Re^{-0.331}$, the dashed line is the line $l = 2.391Re^{-\frac{3}{11}}$.

illustrate this behaviour, on table 1(*a*) is the vortex position at $t = 0.94$ for several Reynolds numbers; on table 1(*b*) is the vortex position at various times in the interactive regime for $Re = 44000$.

It is of interest at this stage to analyse the shear-layer interaction regime depicted on figures 9 and 11 in more detail. Elliott *et al.* (1983) speculate that the next stage in the boundary-layer breakdown phenomena is the development of a streamwise lengthscale $O(Re^{-\frac{3}{11}})$ which develops on a timescale of $O(Re^{-\frac{2}{11}})$; the vertical scale in this scenario is $O(Re^{-\frac{3}{11}})$ as well. To determine whether the present calculations are indeed approaching this scenario, the width of the interaction regime, say $l$, is plotted as a function of Reynolds number on figure 15. Estimates of the width of the interaction region have been obtained from the results presented on figures 9 and 11 as well as for results for $Re = 8000$ (not shown). These results have been fitted to a curve of the form $l = cRe^{-b}$; the solid line is the least-squares curve fit result which is $l = 4.796Re^{-0.331}$. This result is broadly in line with the Elliott *et al.* (1983) results and the dashed line in the figure is $l = 2.391Re^{-\frac{3}{11}}$, where the constant is determined by matching with the $Re = 8 \times 10^4$ results. It is clear that the numerical results produce the general trend; however, it appears that the numerical results consistently overestimate the result. It should be noted here that there is some latitude in the choice of where the interaction region begins and ends and care was taken to be consistent for each Reynolds number. Generally, the right-hand boundary of the region was obtained by drawing a vertical line tangent to the main eddy at its right-most point; the left-hand boundary was estimated to be to the left of the kink in the

streamlines at the top of the main eddy. At present, detailed calculations are being performed to ascertain the time-scale of the eruption.

## 6. Summary and conclusions

In the present paper, the solution for the boundary layer induced by a convected rectilinear vortex has been computed numerically using interacting boundary-layer theory. Solutions have been presented for Reynolds numbers of 8000 and higher and the results are the first attempt at a description of the subsequent strong interaction between the vortex and the boundary layer which is indicated by the breakdown of the numerical scheme for all Reynolds numbers considered. A novel feature of the present work is the use of the fast-Fourier-transform technique in the streamwise direction which requires no special coding in reversed-flow regions as in Doligalski & Walker (1984) and in Henkes & Veldman (1987). The results have been compared with those of classical boundary-layer theory for a Reynolds number of $8 \times 10^4$; at this Reynolds number, the computations may be continued beyond the classical boundary-layer result for all vortex strengths studied. Additional calculations (not shown) show that the interacting boundary-layer results collapse to those of non-interacting theory (i.e. Doligalski & Walker 1984) at about a Reynolds number of $8 \times 10^5$ for the grid sizes considered.

The effect of interaction at $Re = 8 \times 10^4$ is substantial; locally in space, for rather high-strength vortices ($\alpha < 0.55$), the effect is to round the top edge of the eddy which forms under the vortex (figures 3 and 4). A kink appears, however, at a later time and the computations cannot be continued further in time in a manner similar to that described by Doligalski & Walker (1984). The effect of interaction is also local in time; the streamline patterns relative to the vortex in the two cases described just above differ only in the latter stages of the calculations (compare figures 3*c*, 4*b*).

The effect of Reynolds number on the calculations is significant. For $8 \times 10^4 \leqslant Re \leqslant 8 \times 10^5$, the interacting-boundary-layer calculations differ from the asymptotic results only in the very latter stages of the calculations. For $Re > 8 \times 10^5$ the differences between the two solutions are insignificant. Extensive calculations for $2.2 \times 10^3 \leqslant Re \leqslant 8 \times 10^4$ indicate, however, that the results are strongly dependent on Reynolds number; in this Reynolds-number regime a new second-order-accurate scheme originally employed by Napolitano *et al.* (1978) has been adapted to the present work. The calculations could then be continued significantly further on in time when compared with results computed using the simple Veldman scheme (equation (33)).

A major result of the present work is that a tertiary eddy is spawned next to the secondary eddy late in the interaction process. The tertiary eddy initially appears in the form of a side lobe with eventually grows and breaks off the secondary eddy (see figures 9 and 13). This occurrence is similar to that observed by Walker *et al.* (1987) for the case of a vortex ring. The vorticity of the tertiary eddy is of the same sign as that of the secondary eddy although the configuration of the vortices is not the same as in the vortex ring problem.

The presence of interaction also allows the formation of a shear layer directly above the recirculating eddy spawned by the parent vortex, which is not observed in the classical boundary-layer calculations of Doligalski & Walker (1984). The formation of this shear layer appears to be crucial to the description of the next stage in the interactive process. The streamwise length of this region (for $\alpha = 0.2$) is about $Re^{-0.331}$, in broad agreement with the theoretically postulated interactive process

described in Elliott *et al.* (1983). In this regard, the present calculations appear to be illustrative of the early stages of the violent interaction process between the boundary layer and the inviscid flow which occurs in large-scale unsteady separation. However, a full description of the interaction phase remains elusive. Moreover, the timescale of the interaction (i.e. $t-t_s = O(Re^{-\frac{2}{11}})$ from Elliott *et al.* (1983) is not evident from the present calculations and must await further study.

It should also be said that the present calculations support the view of Doligalski & Walker (1984) that the boundary layer undergoes an unsteady separation process (i.e. separation meaning the appearance of a closed recirculating eddy within the boundary layer) which is consistent with the Moore–Rott–Sears model (Sears & Telionis 1975). The incorporation of interaction does not significantly modify the process by which the eddy appears; however, it does change the time of appearance and subsequent development of the flow depending on the value of the Reynolds number.

Lastly, it should be pointed out that Tollmien–Schlichting waves have not been seen in any of our calculations. Although it is difficult to say why this is so, it may be that use of the FFT in the present problem suppresses these waves. Another possibility is that the present flow evolves on an $O(1)$ timescale, whereas TS waves appear over a timescale of $O(Re^{-\frac{1}{4}})$.

The authors are grateful for helpful discussions of this work with Professor J. D. A. Walker and Professor O. R. Burggraf and to the referees for their insightful comments. The authors are also grateful to Professor Cunzhen Zhang of Tsinghua University who prepared the figures for the results of §5. One of the authors (A.T.C.) is also grateful to the Pittsburgh Supercomputing Center and the Ohio Supercomputer Center for time to perform some of the calculations presented in this work. This paper is dedicated to A. T. Conlisk, Sr.

*Note added in proof.* It has recently been suggested to one of the authors (A.T.C.) by F. T. Smith that the solutions presented here may be moving toward a breakdown similar to that described in his paper (Smith 1988). Indeed, calculations being done presently (Conlisk 1989), which focus on the time evolution of the pressure gradient and the pressure, clearly show evidence of a presure gradient spike which may be reminiscent of the 'moderate breakup' described by Smith. It is unclear, however, if the calculations are far enough into the interactive regime to correspond precisely to the 'breakup' described. It also seems that the solutions presented in this paper are leading to a breakdown reminiscent of what Smith & Burggraf (1985, p. 38) refer to. Finally, it should be noted that Peridier, Smith & Walker (1988) have also presented calculations for the classical boundary layer in a Lagrangian coordinate system for a vortex in a stagnant fluid and were able to continue the calculations until the singularity in the displacement thickness forms. Indeed, there is evidence to suggest that Lagrangian methods may be superior to the Eulerian methods used in the present problem.

## REFERENCES

BURGGRAF, O. R. 1982 Interacting boundary layer solutions for laminar separated flow past airfoils. *NASA Rep.* NS61622.

BURGGRAF, O. R. & DUCK, P. W. 1982 Spectral computation of triple deck flows. In *Numerical and Physical Aspects of Aerodynamic Flows* (ed. T. Cebeci), p. 145. Springer.

BURGGRAF, O. R., RIZZETTA, D., WERLE, M. J. & VATSA, V. N. 1979 Effect of Reynolds number of laminar separation of a supersonic stream. *AIAA J.* **17**, 336.

CONLISK, A. T. 1989 The pressure field in intense vortex/boundary layer interaction. *AIAA*-89–0293

COOLEY, J. W. & TUKEY, J. W. 1965 *Maths Comput.* **19**, 297.

DAVIS, R. T. & WERLE, M. J. 1982 Progress in interacting boundary layer computations at high Reynolds number. In *Numerical and Physical Aspects of Aerodynamic Flows* (ed. T. Cebeci), p. 187. Springer.

DOLIGALSKI, T. L. & WALKER, J. D. A. 1984 The boundary layer induced by a convected rectilinear vortex. *J. Fluid Mech.* **139**, 1.

DUCK, P. W. & BURGGRAF, O. R. 1986 Spectral solutions for three dimensional triple-deck flow over surface topography. *J. Fluid Mech.* **162**, 1.

ELLIOTT, J. W., COWLEY, S. J. & SMITH, F. T. 1983 Breakdown of boundary layers: (i) on moving surfaces; (ii) in self-similar unsteady flow; (iii) in fully unsteady flow. *Geophys. Astrophys. Fluid Dyn.* **25**, 77.

HARVEY, J. K. & PERRY, F. J. 1971 Flowfield produced by trailing vortices in the vicinity of the ground. *AIAA J.* **9**, 1659.

HENKES, R. A. W. M. & VELDMAN, A. E. P. 1987 On the breakdown of steady and unsteady interacting boundary layer description. *J. Fluid Mech.* **179**, 513.

MILNE-THOMPSON, L. M. 1960 *Theoretical Hydrodynamics*, 4th edn. Macmillan.

NAPOLITANO, M., WERLE, M. J. & DAVIS, R. T. 1978 Numerical solutions of the triple-deck equations for supersonic and subsonic flow past a hump. *David Taylor Naval Ship Research and Development Center, Rep.* AFL 78-6-42.

NELSON, E. S. 1986 Phase averaged measurements of vortex interaction with a solid surface and the breakaway process. M.Sc. thesis, Illinois Institute of Technology.

PERRIDIER, V., SMITH, F. T. & WALKER J. D. A. 1988 Methods for the calculation of unsteady separation. *AIAA*-88-0604.

RILEY, N. 1982 Non-uniform slot injection into a laminar boundary layer. *J. Engng Maths* **15**, 299.

ROSENHEAD, L. 1963 *Laminar Boundary Layers.* Oxford University Press.

SEARS, W. R. & TELIONIS, D. P. 1975 Boundary layer separation in unsteady flow. *SIAM J. Appl. Maths* **28**, 215.

SMITH, F. T. 1988 Finite time breakup can occur in any interacting boundary layer. *Mathematica* (to appear).

SMITH, F. T. & BODONYI, R. J. 1985 On the short-scale inviscid instabilities in flow past surface mounted obstacles and other non-parallel motions. *Aero. J.* **89**, 205.

SMITH, F. T. & BURGGRAF, O. F. 1985 On the development of large sized short-scaled disturbances in boundary layers. *Proc. R. Soc. Lond.* A **399**, 25.

VAN DOMMELEN, L. L. 1981 Unsteady boundary layer separation. Ph.D. thesis, Cornell University.

VAN DYKE, M. 1975 *Perturbation Methods in Fluid Mechanics.* Parabolic.

VELDMAN, A. E. P. 1981 New, quasi-simultaneous method to calculate interacting boundary layers. *AIAA J.* **19**, 79.

WALKER, J. D. A. 1978 The boundary layer due to a rectilinear vortex. *Proc. R. Soc. Lond.* A **359**, 167.

WALKER, J. D. A., SMITH, C. R., CERRA, A. W. & DOLIGALSKI, T. L. 1987 Impact of a vortex ring on a wall. *J. Fluid Mech.* **181**, 99.